Invited Articles

Experimental adventures in variable-density mixing

Kathy Prestridge*
Los Alamos National Laboratory, Los Alamos, New Mexico 87545, USA

(Received 22 June 2018; published 21 November 2018)

Variable-density mixing occurs in the ocean and atmosphere, inertial confinement fusion capsules, stars, and many industrial processes. Our team studies mixing at the laboratory scale, with the goal of extending our understanding to larger and smaller length scales and into multiphysics regimes that include such physics as chemical and thermonuclear reactions and high-energy density plasmas. I will provide examples of studies from Los Alamos in variable-density mixing in multiple regimes, including shock-driven mixing, subsonic mixing, and high-energy density (HED) plasma mixing. In all cases, the density differences of the mixing fluids are at least double, making the mixing well outside regimes covered by the Boussinesq approximation. In these flows, we have discovered time-dependent mixing phenomena, asymmetries in mixing and distribution of turbulent kinetic energy, and interscale energy transfer driven by the mean flow that moves energy from small to large scales via eddy stretching. We have improved our physical understanding by implementing diagnostics such as particle image velocimetry and planar laser-induced fluorescence in challenging, shock-driven flow regimes. Our experimental studies and physical understanding benefit from collaborations with colleagues studying turbulence modeling and performing validation simulations, and these collaborations push us to further improve our experimental platforms and diagnostics.

DOI: 10.1103/PhysRevFluids.3.110501

I. INTRODUCTION

Explosions are phenomenologically exciting multiphysics problems, and some of the most exciting explosions occur in nature. Type Ia supernovae are caused by exploding white dwarf stars, and in April 1987, the Kuiper Airborne Observatory captured the explosion of supernova 1987a, pictured in Fig. 1(a). The structure of the debris in 1987a is caused by the Richtmyer-Meshkov (RM) instability, where perturbations in density are amplified by the explosion and shock wave.

The Cassiopeia A supernova [pictured in Fig. 1(b)] is also a type Ia supernova, and Chandra x-ray images show elements (different colors in the image) that started out in the core of a white dwarf, such as iron and silicon, being ejected far from the core in the remnant. Such an ejection of iron and silicon is pictured in the top left of the Cas A image, where orange and greenish material ejections are breaking the overall symmetry of the explosion. Simulations of type Ia explosions show that the remnant structure and element composition and location are strongly dependent upon asymmetries in ignition and detonation, making the full time evolution of the explosions difficult to predict [1].

Astrophysicists rely on observations, such as those in Fig. 1, that are necessarily limited in their spatial and temporal resolution. Astrophysical phenomena, such as convection in stars and supernovae, occur at very large length scales, with timescales ranging from hundreds of years for convection to seconds for ignition and explosion. Given the strong dependence on initial conditions and other flow conditions, it is very important to have mixing models that will make

*kpp@lanl.gov; extremefluids.lanl.gov

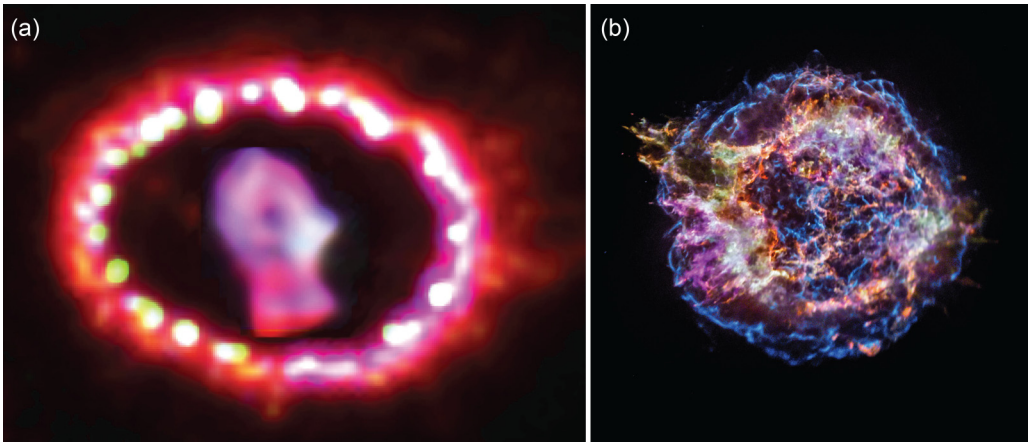

FIG. 1. (a) Supernova 1987a remnant from the Hubble Space Telescope showing a bright ring of debris illuminated by x rays. Shocks from the explosion are heating the debris and making it glow. Image credit: National Aeronautics and Space Administration (NASA), European Space Agency (ESA), and P. Challis. (b) Cassiopeia A supernova remnant x-ray image showing shock wave (blue) and various elements, including sulfur (yellow), silicon (red), calcium (green), and iron (purple). Image credit: NASA, Chandra X-Ray Center (CXC), and Smithsonian Astrophysical Observatory (SAO).

under-resolved simulations more predictive. Our goal is to provide experimental measurements for model development that inform hydrodynamic mixing in these under-resolved flows that exhibit many types of fluid instabilities working in concert, including Kelvin-Helmholtz (KH), Rayleigh-Taylor (RT), and Richtmyer-Meshkov (RM).

At another extreme of length scales and timescales are manmade implosions inside inertial confinement fusion (ICF) capsules at the National Ignition Facility (NIF). The implosions are measured in nanoseconds, and the capsules are only about a millimeter in diameter, as pictured in the schematic in Fig. 2(a). Initial thought on ICF implosions was that indirect drive (via hohlraum) would reduce sensitivities to hydrodynamic instabilities compared to direct laser drive [2]. However, many experiments and calculations since Lindl's review in 1995 have shown that there are multiple types of perturbations caused by the hohlraum (indirect) drive and that the fuel in an imploding ICF capsule is diluted through several different hydrodynamic instabilities and engineering features.

Figure 2(b) shows the effects of engineering features in the capsule. The gas for the ICF capsule is inserted with a fill tube, and the capsule is held in place with a "tent" structure. The effects of the fill tube and tent on the implosion are shown in the x-ray image in Fig. 2(b). The fill tube reduces the

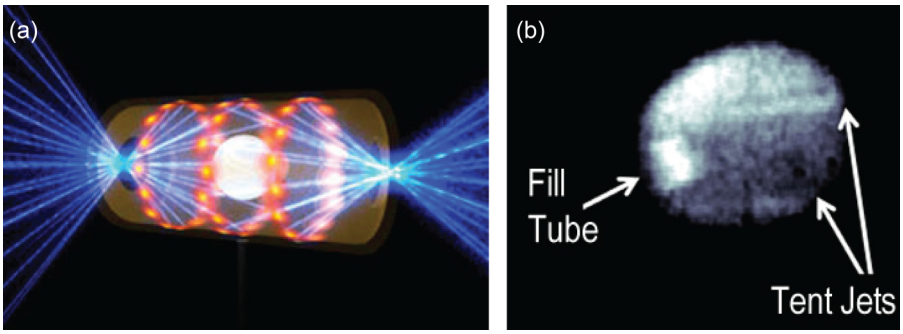

FIG. 2. (a) ICF capsule showing gold hohlraum and laser paths. (b) X-ray microscope image of a capsule imploding at NIF showing perturbations caused by the tent support structure and the gas fill tube [3].

overall compressibility of the fuel during the implosion because fill tube material jets into the center of the fuel cavity. The tent introduces perturbations onto the ablation front of the capsule, causing ablator material to be entrained deep into the hot spot of the capsule. High-resolution simulations are needed to resolve engineering features, and two- and three-dimensional (2-D, 3-D) calculations showing the effects of these structures are described by Clark *et al.*, where he shows that these engineering features affect the compressibility of the fuel [4]. This has an adverse impact on predictability of the implosions because the fuel is then not following the ideal compression adiabat that is modeled in the simulations.

ICF capsules are small, spherical, and imploding, so diagnostics provide limited information about mixing structures. When high-resolution calculations are performed, validation with experimental data does not always resolve modeling issues. An example of an unresolved physics issue, put forward by Thomas and Kares [5], is the idea that turbulence inside the fuel hot spot of an imploding ICF capsule suppresses ignition. They compared 1-D, 2-D, and 3-D calculations with increasing spatial resolution, up to 0.05 μm for the 3-D calculations. Their conclusion was that that the implosion's converging geometry, combined with shear, leads to instabilities that drive turbulence in the hot spot. Experimental measurements of mix of ablator material via x-ray emissions from the hot spot found that drive asymmetries disturb the fuel [6]. However, because of the experimental resolution in a converging capsule geometry, it is impossible to diagnose the level of turbulence in the hot spot.

Subsequent calculations stipulated that the hot spot is viscous, causing the flow in the hot spot to not be turbulent [7]. Weber *et al.* used a model of physical viscosity in their simulations. They found that if viscous effects are neglected (as with Thomas and Kares), the hot spot shows a turbulent kinetic energy (t.k.e.) cascade. But, when viscosity is modeled, the hot spot has a Reynolds number between 10 and 100, and viscosity damps small-scale mixing. They find that the t.k.e. in the hot spot is caused by the initial shock waves, although most of this is dissipated by viscosity. The other source of t.k.e. is the inner surface of the high-density fuel pushing material in front of it during stagnation. Because this energy is long wavelength, it is not damped as well by viscosity. This long-wavelength effect introduces additional complications, because they need 3-D simulations to resolve. Hydrodynamic instabilities seeded by long-wavelength asymmetries cannot be properly captured by reduced-dimension simulations [8], and 2-D calculations bring additional uncertainties when they do not resolve the tent supports [9].

In high-energy density conditions, often dynamic material behavior and equation of state properties, such as viscosity, are not well understood. Conflicts involving numerical predictions and integrated experimental measurements in complex flows then cannot be resolved, especially given measurement uncertainties and model limitations. This drives us to incorporate better physical models into simulations to reduce uncertainties and to improve experimental diagnostics that can feed into more accurate models. High-resolution measurements of reduced-physics experiments or DNS in simplified flow conditions can provide insight into important pieces of physics and guide us in how to develop models that will capture those physics. Unfortunately, for the complex flows in astrophysics or ICF, the flow is not only multiphysical but also time dependent. In many cases, flow predictions are wrong, but we do not know why. It is the quest to understand the physics and improve our simulation capabilities that drives our experimental work at Los Alamos. The following sections describe experimental research into shock-driven (Richtmyer-Meshkov) variable-density mixing, subsonic variable-density mixing, and experiments that study shear, Richtmyer-Meshkov, and other instabilities in flows approaching high-energy density plasma conditions.

II. VARIABLE-DENSITY MIXING

Flows with shocks are very difficult to diagnose because of the low shot rates at shock tube facilities, the convection speed of the mixing region, and the need for high-speed diagnostics. Because of these issues, one of our experimental foci has been on variable-density mixing in a subsonic regime, and we built an open-circuit wind tunnel to study mixing in different configurations. The Turbulent Mixing Tunnel (TMT) is pictured in Fig. 3, in the Turbulence Laboratory at Los Alamos, along

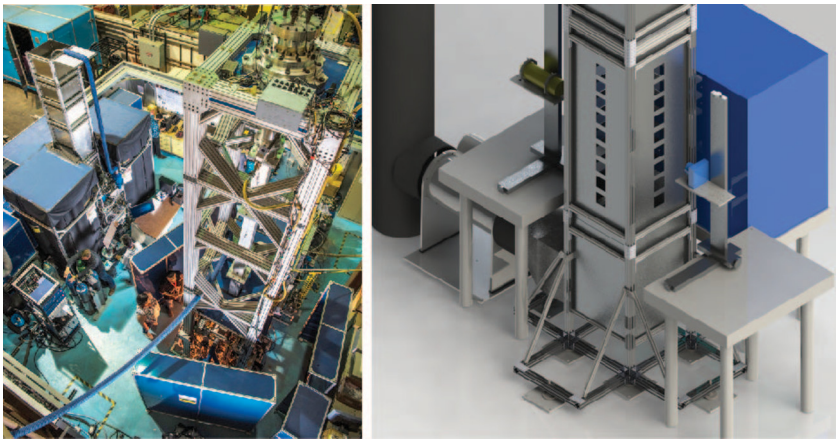

FIG. 3. Turbulence Laboratory at Los Alamos National Laboratory (photo) with Turbulent Mixing Tunnel (TMT) in the left and the Vertical Shock Tube (VST) on the right. Detailed rendering of TMT showing test section in figure on the right.

with the Vertical Shock Tube. Round jet experiments with coflow in the TMT have allowed us to compare Boussinesq and non-Boussinesq mixing in a simplified geometry [10]. Using combined particle image velocimetry (PIV) and planar laser-induced fluorescence (PLIF), we were able to make thousands of measurements of the flow at different downstream locations, providing a large data set to study the mean flow properties and turbulence behavior [11]. Instantaneous snapshots from the two jets, showing three different downstream locations, are shown in Fig. 4.

The spatial resolution of the experiments (about 12η) and the large number of realizations have allowed us to make great insights into non-Boussinesq mixing. Our approach was to first look at single-point turbulence quantities and turbulent kinetic energy budgets. Although the single-point statistics are not always helpful in understanding mixing, a 2-D field allows examination of the spatial variance across the mixing region, so mixing mechanisms can be better understood. In the near field, the jet behaves much like a shear layer. In variable-density shear layers, we expect to see asymmetrical mixing, skewed toward the lighter side of the layer [12], and we observe this in the near-field, shear-dominated region of the variable-density jet.

Understanding mixing in variable-density flows involves looking at the density and velocity fields simultaneously, and if experiments are limited to only one quantity or the other, conclusions about mixing can be significantly different. For example, jet spreading rates are the same for the Boussinesq case whether looking at mass or volume fraction, but mass and volume fraction spreading rates are different in the non-Boussinesq case. And when looking at the velocity profiles, the spreading rates are different and slightly lower in both cases, but the air jet always spreads faster than the SF_6 jet.

In the non-Boussinesq jet, values of turbulence quantities such as the Reynolds stresses are reduced when variable-density effects are included (e.g., Reynolds-averaged quantities are larger than their Favre-averaged counterparts). This difference is important if comparisons of turbulence intensities, turbulent kinetic energy, or other values are being made to experiments where density and velocity are not measured together.

A. The strange behaviors of variable-density turbulence

An exciting discovery in our variable-density jet experiments was negative production of t.k.e. near the dense jet centerline at both of our downstream measurement stations. Our initial analysis of this behavior was done using single-point turbulence statistics to look at what mechanisms might be driving the negative production in the variable-density jet. We found that production in the dense jet was equally influenced by gradient stretching and turbulent mass flux. Axial gradient stretching

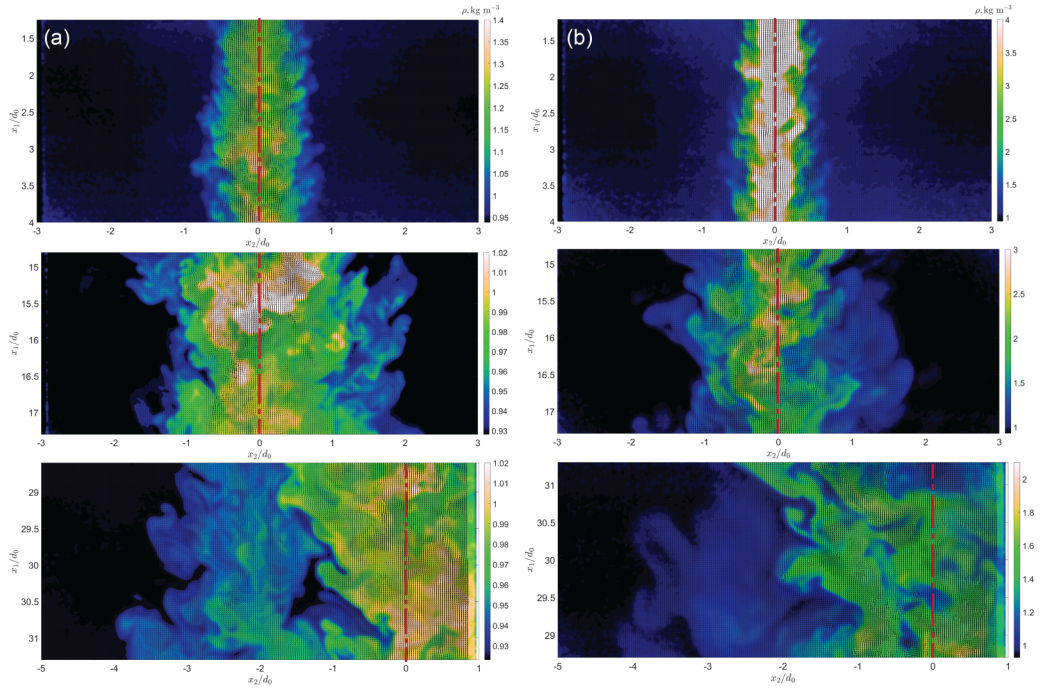

FIG. 4. Velocity and density fields at various downstream locations (x_1/d_0) for (a) air jet and (b) SF_6 jet. Density legends are included on each image because ranges are adjusted for downstream mixing conditions, and the jet centerline is marked in each figure with the red vertical lines. Images are from experiments reported by Charonko and Prestridge [11].

was significantly lower in the dense jet, causing negative net production. There are also significant effects on advection in variable-density flows, with total advection in the variable-density jet almost zero because of counteracting radial and axial effects. The low advection in the dense jet causes more energy to be transported inward, creating significantly higher turbulent flux compared to the Boussinesq jet [11].

While the mechanisms causing mixing differences can be somewhat discerned using single-point analysis, if we want to understand the length scales at which the negative production of t.k.e. is occurring, we must use a different methodology. This is what motivated the development of a variable-density version of the interscale energy equation of von Karman and Howarth [13,14]. This provides us with a new tool to understand the length scales at which energy transfer is occurring and how this varies between the variable-density and Boussinesq cases.

We discovered that the dissipation mechanisms are similar between the Boussinesq and non-Boussinesq cases, but variable-density effects are present at larger length scales than the Kolmogorov scale. Total interscale energy transfer rate across a scale, r, is the sum of nonlinear (Π) and linear (Π_U) terms in the variable-density Karman-Howarth-Monin equation (VDKHM), namely,

$$\Pi + \Pi_U = \frac{\partial \overline{\delta u_k'' (\delta u_i'')^2_\rho}}{\partial r_k} + \frac{\partial \delta \tilde{U}_k \overline{(\delta u_i'')^2_\rho}}{\partial r_k}. \tag{1}$$

Negative values of these divergences indicate energy transfer from large to small scales, while positive values indicate the opposite. The turbulent energy cascade is measured through the Π value, while vortex stretching or compression from the mean flow gradients is measured by Π_U. Close examination of these terms, plus the scale-by-scale energy budgets, reveals that while both jets have forward cascades, the effects of the linear terms are different. The air jet has vortex compression,

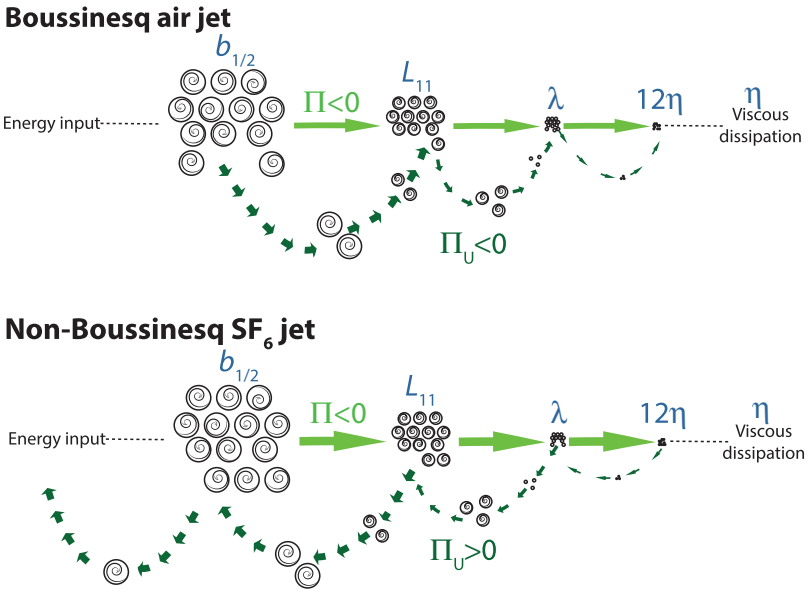

FIG. 5. Energy transfer mechanisms in air (top) and heavy SF_6 jet (bottom) showing the vortex stretching mechanism in variable-density jet that moves energy from smaller to larger scales at all measured length scales of the flow. Size of the arrows is proportional to the amount of energy transfer. Figure adapted from Lai *et al.* [14]

indicated by a negative linear term, that contributes to its forward energy cascade. The heavy jet is different, with vortex stretching, indicated by a positive linear term, retarding the overall energy cascade. These mechanisms are illustrated in Fig. 5.

The relative magnitudes of the interscale energy transfer terms are indicated by the weight of the arrows in Fig. 5. The forward cascade is stronger in the heavy jet, but that is retarded by the vortex-stretching mechanism that moves energy from small to large scales. The net interscale energy transfer for both jets is similar, but these mechanisms may be important in some flows, and increased simulation resolution or subgrid models may need to accommodate these mechanisms in some applications.

There are important consequences of the mechanisms in the variable-density jet illustrated in Fig. 5. The production at the large scales sets the dissipation in the Boussinesq jet, or $P \approx \overline{\epsilon}$, because the interscale energy transfer is negligible in the Boussinesq jet at large scales. In the variable-density case, $-\Pi + P \approx \Pi_U + \overline{\epsilon}$, so energy at scales larger than the Kolmogorov dissipation scale, η, is being removed from the small scales and added to the large scales.

Further studies of these datasets are ongoing to better understand how variable-density effects may be important in subgrid scale models and Reynolds-averaged-Navier-Stokes (RANS) model closures. The magnitude of these effects on larger scale simulations of multiphysics systems, such as ICF capsules or star convection, has to be studied case by case. These effects will be important in Rayleigh-Taylor and Richtmyer-Meshkov mixing, but they will be more difficult to discern because diagnostics and flow setup are much more difficult in those flows.

III. RICHTMYER-MESHKOV MIXING

A. Quantifying mixing in RM flows

Experimental work on RM mixing at Los Alamos has been driven by the need to improve our diagnostics to be able to measure turbulence quantities and by the need to control initial conditions.

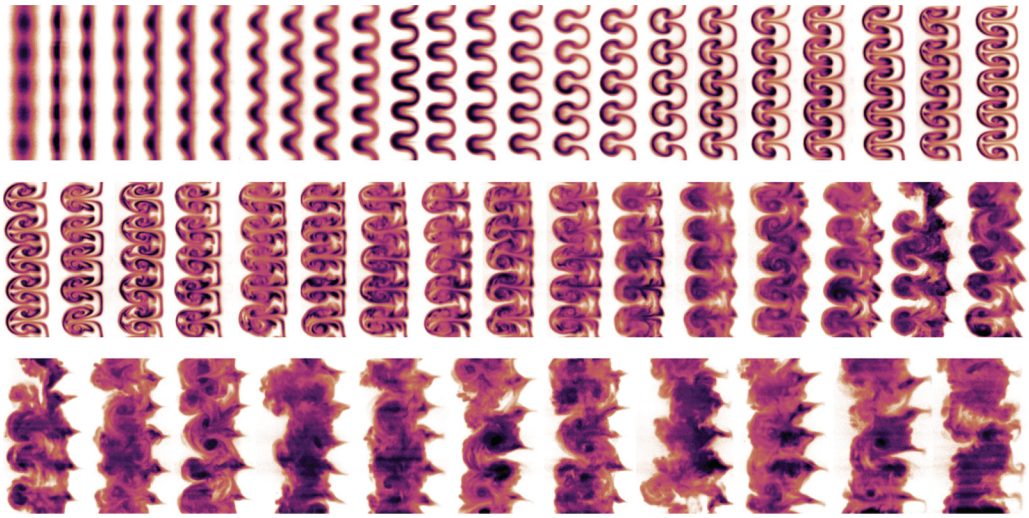

FIG. 6. PLIF images of heavy gas curtain of SF_6 surrounded by air (top left) accelerated by a Mach 1.36 shock wave (moves from left to right). Time series shows initial condition and compression by the shock, and extends out to 1.7 ms after the initial shock of the curtain. Figure is created from experiments reported in Orlicz *et al.* [23].

The importance of the diagnostics is obvious, but the need to control the initial conditions was not always as obvious as it is today [15]. Shock tubes are usually used for RM experiments in laboratories, with early experiments using shadowgraphy or schlieren to measure the mixing width of the shocked gas interface with time. Two recent review articles discuss both RM and RT experiments, simulations, and modeling in very extensive detail, for the interested reader or new student [16,17]. In the decades since the first shock tube experiments at Los Alamos, we have made great improvements in flow control and measurements, giving us new insights into the world of shock-driven mixing.

The horizontal shock tube facility (HST) was set up to study RM for many decades until it was converted to study shocked multiphase flows in 2013 [18,19]. During the last decade of its operation, we were able to make some amazing observations about shock-driven mixing in the gas curtain configuration, where a layer of heavy SF_6 gas surrounded by air was accelerated by shock waves ranging from Mach 1.2 to 1.5 [20].

The path to insight in RM mixing involves capturing the time evolution of a shocked mixing zone that convects along the test section at about 100 m/s for a Mach 1.2 shock. One way watch the convecting mixing zone is to move the light source and camera at the convection speed alongside the shock tube, if they are fast enough in pulse rate and framing frequency. The solution for our experiment was to take images at two measurement stations and splice together the time evolution of the flow from separate experiments. Each measurement station has three laser pulses and two cameras, for simultaneous PIV and acetone PLIF. This image compilation technique requires careful control of the initial conditions, and multiple shots at a given time after shock are necessary to understand the stochastic mixing at the smaller scales as the flow develops in time. The reproducibility of the flow at any given time can be studied, but the cost of repeated experiments is high because the turnaround time for shock tubes is tens of minutes at best.

The first step in quantifying mixing from a time series is to understand the growth rate of the layer by measuring the integrated mixing width. For a gas curtain with a single-mode perturbation, such as that pictured in Fig. 6, the early-time nonlinear growth of the shocked layer can be described using a modified point vortex model [21]. However, when the flow is shocked again by the shock reflected off the end wall of the shock tube, the growth rate increases substantially, and the flow can quickly becomes turbulent. A study of mixing evolution after reshock based on changing reshock timing

shows that mixing transition is strongly affected by the flow structure at reshock [22]. This pattern is being studied in new HED experiments at NIF, described in more detail at the end of Sec. IV.

The mixing in the complex structures shown in Fig. 6 can be quantified in several ways. While the growth rate is useful for zeroth-order comparisons with simulations, one number (the curtain width) to describe the complexity of mixing that is occurring in the mixing zone is really not sufficient. There are many questions that can be asked about shock-accelerated variable-density mixing, such as the following: How do initial conditions affect the development of the flow? How can mixing transition be described, and what is its dependence upon incident shock Mach number, initial conditions, and the density ratio between the mixing gases (Atwood number)? What is the nature of the turbulence, and how does it evolve in time? Many of these questions arise directly from the unsteady nature of RM flows, and understanding how this turbulence varies from steady, isotropic, homogeneous turbulence is valuable for modeling and predictive capabilities.

B. Calculating turbulence quantities in RM flows

Our team spent many years characterizing mixing using PLIF images, and some insight was gained regarding nonuniformity in the mixing layer and the importance of validating against flow features much smaller than the mixing width to compare with numerical predictions [23–25]. We were also able to understand the vorticity in the flow using PIV diagnostics to measure the large-scale vorticies generated by shock passage [26,27] and to understand the secondary instabilities that drive mixing transition [28]. However, it was not until our PIV diagnostics improved in spatial resolution and could be run simultaneously with the PLIF that we could more deeply interrogate variable-density mixing and turbulence. In implementing PIV in shock-driven flows with Mach number as low as 1.7, if tracer particles for PIV are put in one gas and not the other, the density difference between the seeded and unseeded flow can set up instabilities that mimic RM [29], so seeding of both gases is optimal.

Looking at turbulence in shock-accelerated flows calls for careful description of the method of averaging to determine mean and fluctuating quantities from the individual or very few realizations of the flow are available for averaging. Quantities derived from single realizations will often have higher peaks or more extreme fluctuations, as shown by measurements of the density specific-volume covariance plots in Fig. 7(a) [30]. Orlicz *et al.* also showed that calculating turbulent kinetic energy from instantaneous snapshots before the flow has transitioned will result in artificially high levels of t.k.e. compared to ensemble averages (see their Fig. 6). This discrepancy disappears later in time, after the flow has gone through a mixing transition [31].

The first measurements that we were able to perform where we could calculate turbulent mass flux were reported by Balakumar *et al.* [21]. The spatial variation of the turbulent mass flux across the mixing region was compared to the density throughout the layer after reshock, when the flow was generally viewed as fully developed, as shown in Fig. 7(b). The spanwise turbulent mass flux was nonzero, however, indicating that the flow was not fully mixed [30].

The important part of this observation is that it was not foreseen by looking at pictures of the density fields alone. For the first time, we were able to measure the magnitude of the variable density effects in shocked flows, and Reynolds stress components across the mixing layer showed that the flow is dominated by the mean density term, with the mass flux and triple correlation terms being orders of magnitude smaller. One question that often comes up in shock-driven flows is the degree of isotropy. Looking only at the velocity fluctuations, the flow appears to tend toward isotropy in the velocity field [31]. This can be the case even when there is significant anisotropy in the density field.

Measurements from these experiments compare well with gas curtain simulations of Shankar and Lele [32]. Asymmetries in mixing and turbulent mass flux were also explored and confirmed experimentally with different initial conditions [22,33]. As with the variable-density jet measurements given by Charonko and Prestridge [11], Tomkins *et al.* [34] also found that using the Boussinesq equations (Reynolds averaging) will overpredict the mass flux in certain parts of the flow [34].

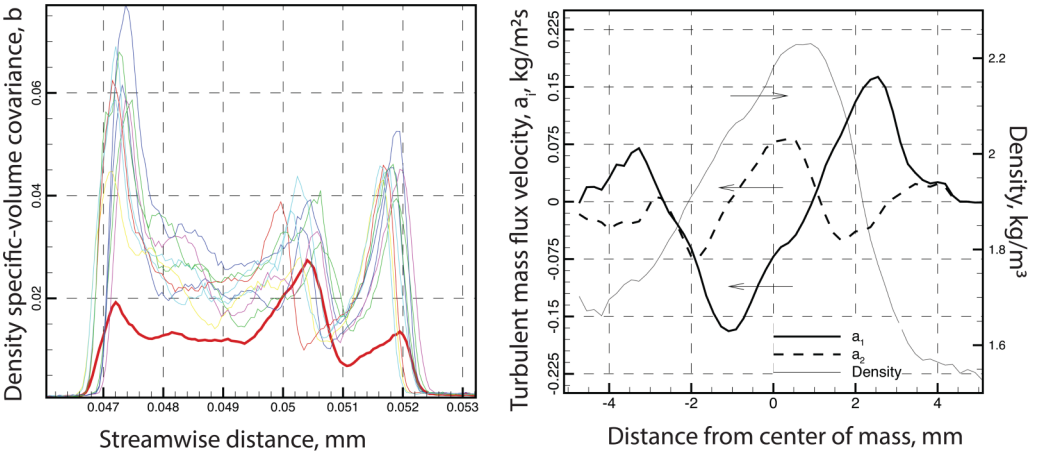

FIG. 7. Density specific-volume covariance in gas curtain experiments determined from instantaneous realizations through the mixing region at 515 μs after shock and from an ensemble (thick red line), showing differences based on averaging techniques used. Turbulent mass flux in streamwise (a_1) and spanwise (a_2) directions compared to density profile in reshocked gas curtain. Figures are derived from experiments described in Ref. [30].

First estimates of the dissipation in RM flows, based on the PIV velocity fields, were estimated by Tomkins *et al.* [34] and used to determine length scales of the flow. This step allowed us to compare RM transitional flow to that predicted for other flows, to find similarities between unsteady and steady turbulent mixing flows. The RM flow was found to generally satisfy the time-dependent mixing transition criterion developed by Zhou *et al.* [35].

C. Mixing transition insights based on Reynolds numbers and length scales

Sometimes, with complex, multiphysics flows, as we see in HED experiments, it is difficult to get measurements of density and velocity, so you have to resort to estimating flow quantities with a lot less information. Because the gas curtain shock tube experiments have density and velocity diagnostics, we can calculate multiple different mixing quantities, see how they vary, and use that information to better understanding the global quantities measured in flows with much lower resolution diagnostics, such as ICF experiments.

We have done some work to compare mean flow and turbulence quantities with the gas curtain experiments, comparing Reynolds numbers and estimates of mixing length scales that use local and global variables. Generally, Reynolds numbers based on global values such as mean flow velocity, mixing width growth rates, or circulation tend to agree with each other [34]. We did not fully understand why Reynolds numbers calculated using local or turbulent values were not consistent between experiments until we performed a detailed study of time-dependent Reynolds numbers with the gas curtain, varying incident Mach number. This work helped us to understand which Reynolds numbers are most useful during what phase of the flow [31]. For example, global-variable Reynolds numbers (based on mix width or circulation) are useful for understanding the early-time development of the flow, when it is dominated by inviscid vortex dynamics, while the turbulent Reynolds number is most useful in discerning differences in the mixing in the late-time part of the flow.

Another problem with unsteady mixing flows is that the physical properties of the mixing materials are continuously changing over time. Time-resolution of measurements is important, and updating physical quantities when calculating flow parameters is critical. Figure 8 from Orlicz *et al.* [31] shows the dramatic changes in mean kinematic viscosity over the course of gas curtain experiments at three different Mach numbers, and these values were used to calculate Taylor microscales over time across

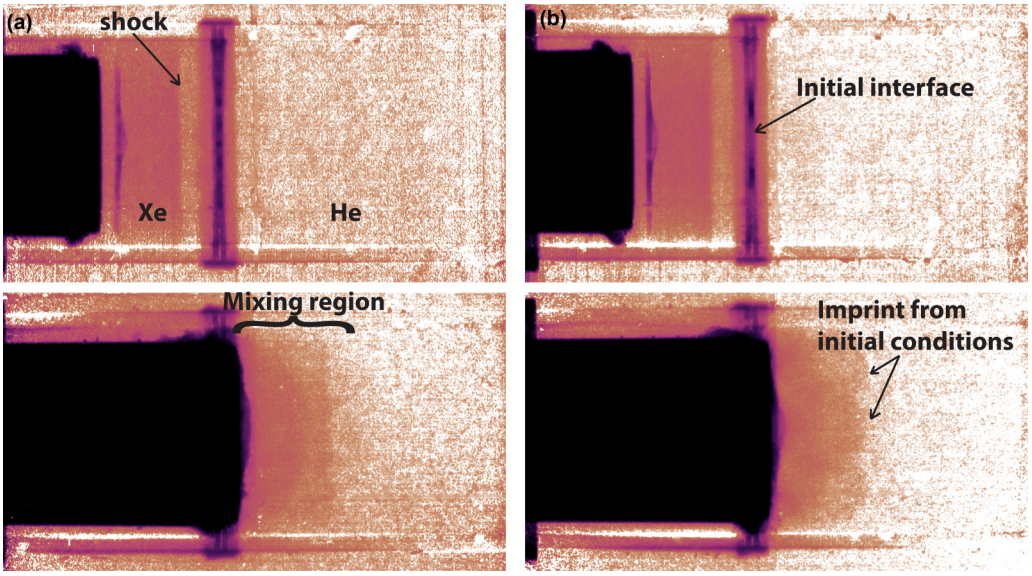

FIG. 8. New experiments using the LANSCE pRad facility, driving a Mach 8.9 (top row) shock into xenon, with different interfaces separating the xenon from helium gas. The initial condition perturbations are (a) 14.8 mm and (b) 8.9 mm. Bottom row shows the mixing region between the xenon and helium about 18 μs after shock acceleration. Imprint of the initial conditions is visible in the mixing region.

the entire mixing region for the three experiments. A change in the Taylor microscale calculated from the density field appears to be a good way to determine mixing transition and is shown in Fig. 16 of that paper [31].

We know we will not be able to measure turbulence quantities yet in a Mach 9 RM experiment that we recently started at the Los Alamos Neutron Science Center (LANSCE) proton radiography (pRad) facility. A powder gun drives a 40-mm diameter sabot into a plastic shock tube that is about 44 mm in diameter, pictured in Fig. 8.

The analysis of the pRad RM experiments is ongoing. We can see the mixing region clearly in the radiographs, and we have a 31-frame time series of the events, from shock impact to mixing. We will use these to determine the mixing width growth versus time as a function of the initial conditions, much in the way that laboratory-scale shock tube experiments use schlieren to study mixing.

IV. HIGH-ENERGY DENSITY EXPERIMENTS

Understanding the effects of different physics, such as fluid instabilities, fill tube perturbations, and convergence, are challenging in an HED implosion. By simplifying the geometry to a shock tube platform, we gain several advantages. Simplified platforms allow specific physics problems to be isolated, cleaner lines of sight for diagnostics, and greater control over initial conditions and the dynamic shock behavior within the tube. An example is preheat, when the material properties and sometimes even shape change because it is heated up even before the dynamic experiment begins. This provides a big challenge from a dynamics and an equation of state perspective. With a simplified geometry and careful choice of materials, preheat can be controlled and/or observed.

A platform was developed at Los Alamos to study the effects of shear-driven mixing in an HED environment [36]. The configuration of the shock-shear platform is shown in Fig. 9. The design is set up in a shock tube configuration, and the counterpropagating shock setup causes pressure and velocity balances at the center of the test section. This creates simplified flow conditions that make it easier for experimental results, where velocities cannot yet be measured, to be compared to models.

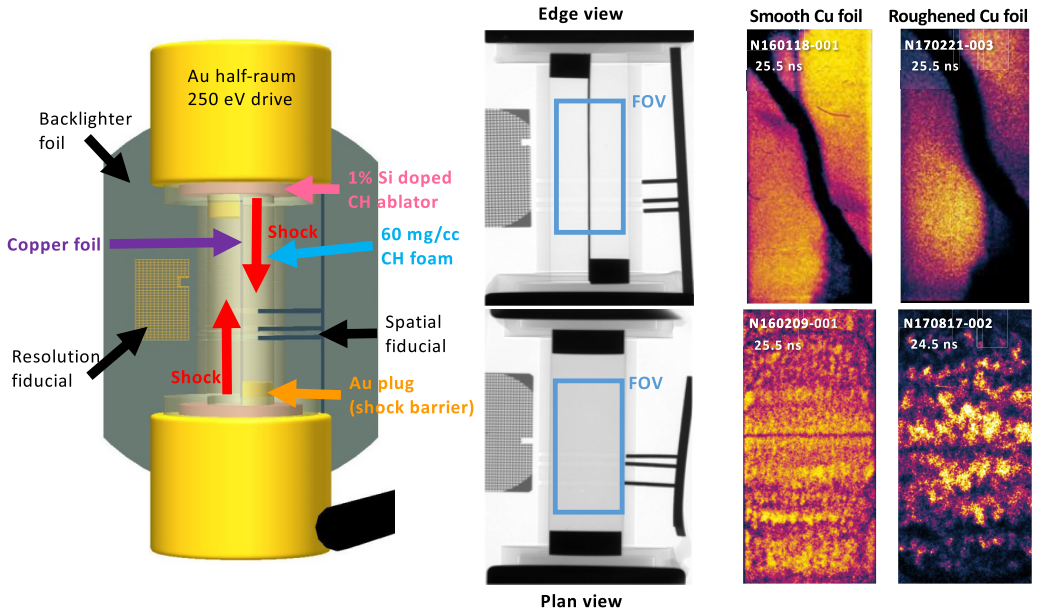

FIG. 9. NIF Shear platform experiments comparing evolution of two different types of initial conditions at 25 ns. The shock tube is approximately 5.7 mm long. The initial conditions are changed by modifying the surface roughness of the copper tracer foil. Kelvin-Helmholtz shear rollers can be seen in the smooth copper plan view. The rough initial conditions did not develop strong rollers, but the mixing zone width grew faster. Figures adapted from Flippo *et al.* with permission [37].

The HED shock tube setup in Fig. 9 is a bit different than a gas- or gun-driven tube because it is much shorter. This is due to the way the shock is created at the ends of the tubes using the gold halfraums. ICF capsules use a gold cylindrical hohlraum to surround the capsule, while the HED shock tube uses two halfraums at each end of the shock tube to focus the laser energy. Lasers are shot into both ends of the hohlraum, generating x rays that drive the capsule implosion. The shock tube configuration for the shear platform uses gold halfraums at each end of the tube to generate the x rays that drive the shocks. The heat created when the shocks are generated preheats the materials in the tube, causing them to become ionized fluids before they are accelerated by the shock.

Shocks propagate down the tube from both directions simultaneously, but small gold plugs are set on opposite sides to delay shock propagation. This creates a shock counterflow in the test section of the shock tube, and the growth of the copper layer under shear flow conditions can be measured using x-ray radiography from both edge and plan directions relative to the copper foil layer.

New platforms are first tested out on the University of Rochester's OMEGA laser to understand the effects of preheat and shock timing. Then, the platforms are often modified, improved, and shot at the NIF at Lawrence Livermore National Laboratory (LLNL). Initial studies of the shock-shear platform at OMEGA showed that the growth of the shear layer, as indicated by tracer materials, is increased with increased roughness perturbations in the tracer layer [38]. Time series of the growth were patched together from separate experiments, since two radiographs per shot were available.

In the shear experiments at the NIF, pictured in Fig. 9, both side and plan views of the instability were captured for rough and smooth initial conditions on the copper foil between the two shear layers. The smooth initial conditions have a surface rms perturbation on the copper tracer foil of approximately 0.3 μm, and the rough initial conditions are 2.25 μm. The smooth initial conditions showed Kelvin-Helmholtz rollers, while the rougher initial conditions showed mixing without the appearance of coherent structures. The mixing width grows much more quickly for the rough initial conditions. The first observations of KH shear rollers in an HED environment were due to this

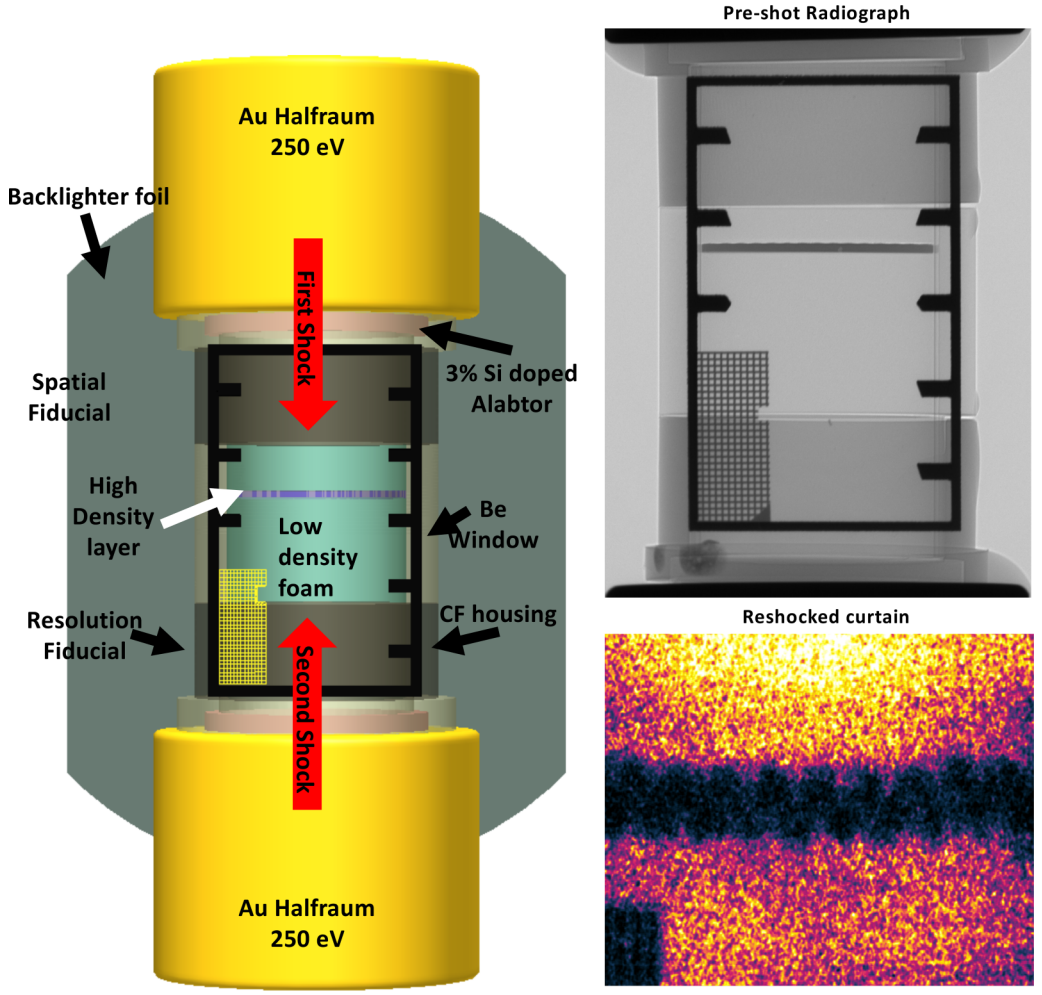

FIG. 10. NIF Mshock platform with schematic, preshot radiograph, and curtain of dense material shown 5 ns after reshock. Reshock occurred 13 ns after first shock. Experiments described in Ref. [39].

simplified flow configuration [37,40,41]. These experiments are being studied to determine how to initialize turbulence models based upon different experimental initial conditions.

By simulating these simplified geometries, turbulence models can be tested in HED regimes to see how well they predict growth rates of instabilities using models developed for continuum flows. Additional platforms to study geometries like the gas curtain experiments and pRad experiments are being developed so that we can make measurements of RT and RM instabilities in a range of flow regimes [42–44]. The gas curtain geometry is pictured in Fig. 10. The Mshock (multiple shock) platform was designed to show shock and reshock, similar to the experiments by Balasubramanian *et al.* [22]. By altering reshock timing, as in the LED experiments, the flow complexity changes and the effects of initial conditions can be studied systematically. Later reshock results in faster mixing rates, and that phenomenology can be studied under much different flow conditions.

V. CONCLUDING REMARKS

Low- and high-energy density fluid dynamics experimental research at Los Alamos is focused on understanding hydrodynamic instabilities, variable-density mixing, and shock-driven mixing in

regimes where the flows can be diagnosed well and where reduced-order physical effects can be studied.

The current state of the art for diagnostics in RM flows is to implement planar PIV and PLIF simultaneously. The implementation of these diagnostics is very difficult, especially for quantitative density measurements. Yet, full understanding of turbulent mixing requires measurement of the out-of-plane gradients to reconstruct the Reynolds stresses of the flow. Extending optical density and velocity measurements to out of plane and 3-D is especially challenging because of the nonuniform index of refraction in mixing, variable-density flows. Possible steps forward can be made in spatial and temporal resolution using high-speed scanning and stereo techniques, but the equipment needed can be cost prohibitive.

Understanding and characterizing the effects of initial conditions have always been challenging for experimentalists. Additional support is needed from numerical physicists to understand the sensitivities of existing models and simulations to changes in initial conditions. This would include the effects of small-amplitude noiselike perturbations and single- and multimode large-amplitude perturbations in two and three dimensions.

Recent directions at Los Alamos have led us to explore how hydrodynamic instabilities scale in high-energy density environments, where continuum approximations are no longer valid. Experiments that mimic low-energy density shock tubes are allowing us to observe and scale instability behavior into the HED regime. Diagnostics in HED flows must be improved so that they can go beyond line-of-sight density measurements. Simplified experiments are also needed to measure material properties such as viscosity and sound speed. Experiments that focus on equations of state of materials under HED conditions would contribute greatly to our understanding of how to scale the flows from the LED parameter space.

Turbulent mixing in applications from astrophysics to inertial confinement fusion is time dependent and can occur in different locations of the flow, affecting ICF capsule fuel compression and white dwarf ignition locations. Unfortunately, we do not know *a priori* when and where in a flow we might need to more precisely resolve and understand the mixing. Experiments can provide new insights in simplified flow configurations, such as our observations of energy transfer from small to large scales via eddy stretching in non-Boussinesq flows, but the larger impact of this physics on complex applications is not clear. Advances will only happen with collaboration among experimentalists, model developers, and numerical physicists, as each new experiment with our facilities and platforms brings us closer to understanding how turbulence and mixing behave in very challenging flow conditions.

ACKNOWLEDGMENTS

Thanks to all members of the Extreme Fluids Team, past and present, and to my colleagues in plasma physics and astrophysics. My collaborations with colleagues on the team, across disciplines, and in modeling and simulation are what keep the research exciting.

[1] D. Kasen, F. K. Ropke, and S. E. Woosley, The diversity of type Ia supernovae from broken symmetries, Nature (London) **460**, 869 (2009).

[2] J. Lindl, Development of the indirect-drive approach to inertial confinement fusion and the target physics basis for ignition and gain, Phys. Plasmas **2**, 3933 (1995).

[3] V. Smalyuk, H. Robey, and S. Johnson, Working to tame disturbances in the NIF force, *NIF Science and Technology News*, December 2017.

[4] D. S. Clark, C. R. Weber, J. L. Milovich, J. D. Salmonson, A. L. Kritcher, S. W. Haan, B. A. Hammel, D. E. Hinkel, O. A. Hurricane, O. S. Jones *et al.*, Three-dimensional simulations of low foot and high foot implosion experiments on the national ignition facility, Phys. Plasmas **23**, 056302 (2016).

[5] V. A. Thomas and R. J. Kares, Drive Asymmetry and the Origin of Turbulence in an ICF Implosion, Phys. Rev. Lett. **109**, 075004 (2012).
[6] T. Ma, P. K. Patel, N. Izumi, P. T. Springer, M. H. Key, L. J. Atherton, L. R. Benedetti, D. K. Bradley, D. A. Callahan, P. M. Celliers *et al.*, Onset of Hydrodynamic Mix in High-Velocity, Highly Compressed Inertial Confinement Fusion Implosions, Phys. Rev. Lett. **111**, 085004 (2013).
[7] C. R. Weber, D. S. Clark, A. W. Cook, L. E. Busby, and H. F. Robey, Inhibition of turbulence in inertial-confinement-fusion hot spots by viscous dissipation, Phys. Rev. E **89**, 053106 (2014).
[8] B. M. Haines, F. F. Grinstein, and J. R. Fincke, Three-dimensional simulation strategy to determine effects of turbulent mixing on inertial-confinement-fusion capsule performance, Phys. Rev. E **89**, 053302 (2014).
[9] C. R. Weber, D. T. Casey, D. S. Clark, B. A. Hammel, A. MacPhee, J. Milovich, D. Martinez, H. F. Robey, V. A. Smalyuk, M. Stadermann *et al.*, Improving ICF implosion performance with alternative capsule supports, Phys. Plasmas **24**, 056302 (2017).
[10] S. Gerashchenko and K. Prestridge, Density and velocity statistics in variable density turbulent mixing, J. Turbulence **16**, 1011 (2015).
[11] J. J. Charonko and K. Prestridge, Variable density mixing in turbulent jets with coflow, J. Fluid Mech. **825**, 887 (2017).
[12] G. L. Brown and A. Roshko, On density effects and large structure in turbulent mixing layers, J. Fluid Mech. **64**, 775 (1974).
[13] T. von Kármán and L. Howarth, On the statistical theory of isotropic turbulence, Proc. Royal Soc. London, Ser. A **164**, 192 (1938).
[14] C. K. C. Lai, J. J. Charonko, and K. Prestridge, A Karman-Howarth-Monin equation for variable-density turbulence, J. Fluid Mech. **843**, 382 (2018).
[15] W. K. George, The decay of homogeneous isotropic turbulence, Phys. Fluids A **4**, 1492 (1992).
[16] Y. Zhou, Rayleigh-Taylor and Richtmyer-Meshkov instability induced flow, turbulence, and mixing. I, Elsevier Phys. Rep. **720–722**, 1 (2017).
[17] Y. Zhou, Rayleigh-Taylor and Richtmyer-Meshkov instability induced flow, turbulence, and mixing. II, Elsevier Phys. Rep. **723–725**, 1 (2017).
[18] A. A. Martinez, G. C. Orlicz, and K. P. Prestridge, A new experiment to measure shocked particle drag using multi-pulse particle image velocimetry and particle tracking, Exp. Fluids **56**, 1854 (2015).
[19] A. D. Bordoloi, A. A. Martinez, and K. Prestridge, Relaxation drag history of shock accelerated microparticles, J. Fluid Mech. **823**, 1 (2017).
[20] K. Prestridge, G. Orlicz, S. Balasubramanian, and B. J. Balakumar, Experiments of the Richtmyer-Meshkov instability, Phil. Trans. R. Soc. A **371**, 20120165 (2013).
[21] B. J. Balakumar, G. C. Orlicz, C. D. Tomkins, and K. P. Prestridge, Simultaneous particle-image velocimetry and planar laser-induced fluorescence measurements of Richtmyer-Meshkov instability growth in a gas curtain with and without reshock, Phys. Fluids **20**, 124103 (2008).
[22] S. Balasubramanian, G. C. Orlicz, K. P. Prestridge, and B. J. Balakumar, Experimental study of initial condition dependence on Richtmyer-Meshkov instability in the presence of reshock, Phys. Fluids **24**, 034103 (2012).
[23] G. C. Orlicz, S. Balasubramianian, and K. P. Prestridge, Incident shock mach number effects on Richtmyer-Meshkov mixing in a heavy gas layer, Phys. Fluids **25**, 114101 (2013).
[24] G. C. Orlicz, B. J. Balakumar, C. D. Tomkins, and K. P. Prestridge, A mach number study of the Richtmyer-Meshkov instability in a varicose, heavy-gas curtain, Phys. Fluids **21**, 064102 (2009).
[25] A. A. Gowardhan and F. F. Grinstein, Numerical simulation of Richtmyer-Meshkov instabilities in shocked gas curtains, J. Turbulence **12**, 43 (2011).
[26] K. Prestridge, P. Vorobieff, P. M. Rightley, and R. F. Benjamin, Validation of an Instability Growth Model using Particle Image Velocimetry Measurements, Phys. Rev. Lett. **84**, 4353 (2000).
[27] K. Prestridge, P. M. Rightley, P. Vorobieff, R. F. Benjamin, and N. A. Kurnit, Simultaneous density-field visualization and PIV of a shock-accelerated gas curtain, Exp. Fluids **29**, 339 (2000).
[28] P. Vorobieff, N. G. Mohamed, C. Tomkins, C. Goodenough, M. Marr-Lyon, and R. F. Benjamin, Scaling evolution in shock-induced transition to turbulence, Phys. Rev. E **68**, 065301 (2003).

[29] P. Vorobieff, M. Anderson, J. Conroy, R. White, and C. R. Truman, Vortex Formation in a Shock-Accelerated Gas Induced by Particle Seeding, Phys. Rev. Lett. **106**, 184503 (2011).
[30] B. J. Balakumar, G. C. Orlicz, J. R. Ristorcelli, S. Balasubramanian, K. P. Prestridge, and C. D. Tomkins, Turbulent mixing in a Richtmyer-Meshkov fluid layer after reshock: Velocity and density statistics, J. Fluid Mech. **696**, 67 (2012).
[31] G. C. Orlicz, S. Balasubramianian, P. Vorobieff, and K. P. Prestridge, Mixing transition in a shocked variable-density flow, Phys. Fluids **27**, 114102 (2015).
[32] S. K. Shankar and S. K. Lele, Numerical investigation of turbulence in reshocked Richtmyer-Meshkov unstable curtain of dense gas, Shock Waves **24**, 79 (2014).
[33] S. Balasubramanian, G. C. Orlicz, and K. P. Prestridge, Experimental study of initial condition dependence on turbulent mixing in shock-accelerated Richtmyer-Meshkov fluid layers, J. Turbulence **14**, 170 (2013).
[34] C. D. Tomkins, B. J. Balakumar, G. Orlicz, K. P. Prestridge, and J. R. Ristorcelli, Evolution of the density self-correlation in developing Richtmyer-Meshkov turbulence, J. Fluid Mech. **735**, 288 (2013).
[35] Y. Zhou, H. F. Robey, and A. C. Buckingham, Onset of turbulence in accelerated high-Reynolds-number flow, Phys. Rev. E **67**, 056305 (2003).
[36] F. W. Doss, J. R. Fincke, L. Welser-Sherrill, E. N. Loomis, and K. A. Flippo, The high-energy-density counterpropagating shear experiment and turbulent self-heating, Phys. Plasmas **20**, 122704 (2013).
[37] K. A. Flippo, F. W. Doss, E. C. Merritt, B. G. DeVolder, C. A. Di Stefano, P. A. Bradley, D. Capelli, T. Cardenas, T. R. Desjardins, F. Fierro *et al.*, Late-time mixing and turbulent behavior in high-energy-density shear experiments at high Atwood numbers, Phys. Plasmas **25**, 056315 (2018).
[38] E. C. Merritt, F. W. Doss, E. N. Loomis, K. A. Flippo, and J. L. Kline, Modifying mixing and instability growth through the adjustment of initial conditions in a high-energy-density counter-propagating shear experiment on OMEGA, Phys. Plasmas **22**, 062306 (2015).
[39] T. Desjardins, C. Di Stefano, E. Merritt, K. Flippo, B. DeVolder, F. Doss, and J. Kline, Mshock, a thin layer Richtmyer-Meshkov instability experiment, *16th International Workshop on the Physics of Compressible Turbulent Mixing, Marseille, France, July 2018* (IUSTI UMR, Marseille, 2018).
[40] F. W. Doss, K. A. Flippo, and E. C. Merritt, Observation and analysis of emergent coherent structures in a high-energy-density shock-driven planar mixing layer experiment, Phys. Rev. E **94**, 023101 (2016).
[41] K. A. Flippo, F. W. Doss, J. L. Kline, E. C. Merritt, D. Capelli, T. Cardenas, B. DeVolder, F. Fierro, C. M. Huntington, L. Kot, E. N. Loomis *et al.*, Late-Time Mixing Sensitivity to Initial Broadband Surface Roughness in High-Energy-Density Shear Layers, Phys. Rev. Lett. **117**, 225001 (2016).
[42] S. R. Nagel, K. S. Raman, C. M. Huntington, S. A. MacLaren, P. Wang, M. A. Barrios, T. Baumann, J. D. Bender, L. R. Benedetti, D. M. Doane *et al.*, A platform for studying the rayleigh-taylor and Richtmyer-Meshkov instabilities in a planar geometry at high energy density at the National Ignition Facility, Phys. Plasmas **24**, 072704 (2017).
[43] C. A. DiStefano, A. M. Rasmus, F. W. Doss, K. A. Flippo, J. D. Hager, J. L. Kline, and P. A. Bradley, Multimode instability evolution driven by strong, high-energy-density shocks in a rarefaction-reflected geometry, Phys. Plasmas **24**, 052101 (2017).
[44] A. M. Rasmus, C. A. Di Stefano, K. A. Flippo, F. W. Doss, J. L. Kline, J. D. Hager, E. C. Merritt, T. R. Desjardins, W. C. Wan, T. Cardenas *et al.*, Shock-driven discrete vortex evolution on a high-Atwood number oblique interface, Phys. Plasmas **25**, 032119 (2018).